Doppler/Angle Coupling and Rejection for Slow-Time Phase Codes in MIMO Radar

Olivier Rabaste, Michel Menelle, Dominique Poullin, Abigael Taylor, Alain Dorey

Doppler/Angle Coupling and Rejection for Slow-Time Phase Codes in MIMO Radar

Olivier Rabaste, Michel Menelle, Dominique Poullin, Abigael Taylor, Alain Dorey
DEMR, ONERA
Université Paris-Saclay, F-91123 Palaiseau, France
firstname.lastname@onera.fr

***Abstract*—In this article, we consider the problem of the Doppler/angle coupling induced by Slow-Time Phase codes in MIMO Radar. We show that such a coupling must be carefully taken into account when clutter rejection is performed for a given Doppler frequency. After studying the simple non-realistic case of one single point-like scatterer and deriving the projector to be used to properly perform the rejection in the Doppler/angle domain, we extend the study to a clutter spread over a continuous angular interval. Simulation results show the efficiency o f the proposed approach.**

***Index Terms*—MIMO radar, Doppler/angle coupling, Slow-Time Phase Code, Clutter rejection**

I. Introduction

MIMO radar has appeared in the early 2000's and rapidly gained tremendous attention [1], [2]. It consists in transmitting different waveforms with the different transmitting antennas of a phased array. A considerable amount of literature has been published on the choice or the optimization of signal waveforms for coherent colocated MIMO radar and of their advantages and drawbacks [3]–[6]. In particular, choosing orthogonal waveforms enables to spread the transmitted energy uniformly in all angular directions. Intrapulse MIMO coding where each antenna transmits a different pulse have often been studying. For such waveforms, orthogonality is not achieved on intrapulse coding but rather over the pulse duration, with the drawbacks of presenting a costly hardware since they require as many Tx generators as transmitted waveforms, and of creating a potentially strong range/angle coupling [7].

Other families of waveforms have thus been considered more recently, that are less costly in terms of hardware. Among these can be found interpulse MIMO coding solutions where the same elementary pulse is transmitted by all antennas and orthogonality is achieved over the pulse train duration by applying a code over the successive pulses. These solutions can be denoted as "Slow-Time Coding" (STC). STC MIMO radars require only one single Tx generator share by all antennas, and the ability to change the transmitted phase or carrier frequency from pulse to pulse and antenna to antenna. Time Division Multiplexed (TDM) MIMO radars [8], where the pulse transmission is switched from an antenna to the other in a random time pattern, belong to this category. Such strategies are however not efficient i n t erms o f S ignal-to-Noise Ratio since only one antenna is excited for a given pulse [9]. To limit that effect, general multiplexed waveforms have been designed where several (at least two) antennas from the array are active during the same pulse, thus improving the SNR [9], [10]. It was shown that that particular coding scheme creates Doppler/angle coupling [9]. Another popular slow-time coding is the DDMA (Doppler Division Multiple Access) [11], that considers Doppler-offset waveforms. This solution can be viewed as a slow-time phase code applied to the transmitted pulse by assuming that the phase rotation due to the Doppler frequency is negligible over the pulse duration.

In this paper, we will consider a general Slow-Time Phase Coding (STPC), where the transmitting antennas are all active at the same time during the whole pulse train transmission, and orthogonality is achieved by use of a phase code that changes the phase from pulse to pulse and antenna to antenna. We will first review the STPC framework, introduce the Matched Filter processing at reception and discuss the Doppler/angle coupling induced by this specific coding scheme. We will in particular show that this Doppler/angle coupling must be carefully taken into account when Doppler rejection is required in the presence of strong clutter echoes: classical Doppler rejection cannot be performed over the sole Doppler domain because of that Doppler/angle coupling, and thus one must perform the rejection in the Doppler/angle domain.

Based on these considerations, we will derive the proper Doppler/angle projector to use for a single point-like scatterer and show that it effectively enables good rejection of the clutter contribution. However in many applications, if clutter scatterers can be considered to be located at the same Doppler hypothesis, as for ground radar with ground echoes at zero-Doppler, or HFSWR (High-Frequency Surface Wave Radar) with Bragg peaks at two specific Doppler values [12]–[14], there contributions are usually spread over a wide angular domain. We thus extend the proposed STPC Doppler/angle projector to a continuous angular interval; funnily enough, we show that when considering a linear transmitting array, this projector involves the Discrete Prolate Spheroidal Sequences (DPSS) [15]. We finally show on simulations that the proposed approach indeed enables the rejection of contributions over a given angular interval at a specific frequency.

This article is organised as follows: in section II, we present the STPC signal model and reception processing. In section III, we consider the rejection of one single point-like scatterer, and then extend the rejection to a continuous angular interval in section IV. Finally we present simulation results in section V.

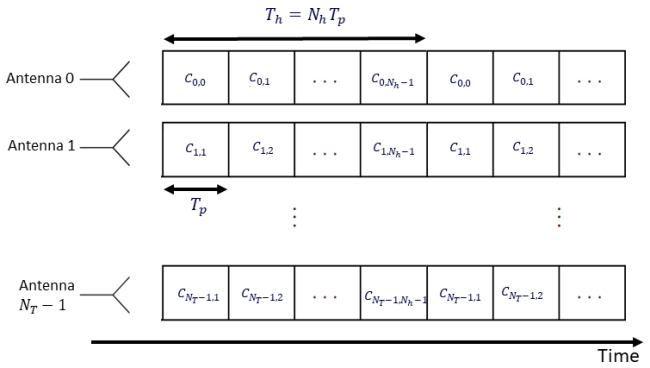

Fig. 1. Slow time phase coding principle for MIMO radar. Orthogonality is achieved over the phase code period $N_h T_p$.

II. Transmitted signal and reception processing

A. Slow-Time Phase Coding and received signal

Let us consider a MIMO transmitting array composed of N_T transmission antennas. In the considered setting, the signal transmitted by each antenna is the same FMCW waveform with an additionnal slow-time phase code that differs from pulse to pulse and from antenna to antenna. In such a setting, the signal transmitted by antenna m can be written as :

$$s_m(t) = \sum_{r=0}^{N_r-1} \sum_{h=0}^{N_h-1} c_{mh} e(t - hT_p - rT_h), \tag{1}$$

where:

- $e(t)$ is the elementary linear frequency modulated (LFM) waveform transmitted by each antenna at each pulse.
- T_p is the pulse duration.
- N_h is the number of chips of the phase code.
- T_h is the duration of the full code, i.e. $T_h = N_h T_p$.
- N_r represents the number of repetitions of the phase code during the overall signal transmission. Thus the total number of transmitted pulses is equal to $N_h N_r$, and the total duration of the transmitted signal is $T_{tot} = N_h N_r T_p$.
- c_{mh} is the phase value for antenna m and time chip h.

For such a STPC code, orthogonality between the signals transmitted by the different antennas is not achieved over the pulse duration but over the full phase code period, i.e. at least $N_h T_p$ here.

If we denote by $\mathbf{x}_m$ the location of the m^{th} transmission antenna in cartesian coordinates, the signal transmitted by the full MIMO array in direction θ is then provided by

$$s_\theta(t) = \sum_{m=0}^{N_T-1} e^{j\mathbf{x}_m^T \mathbf{k}(\theta)} s_m(t) \tag{2}$$

where $\mathbf{k}(\theta)$ is the wave vector in direction θ.

Finally, let us consider that a target is present in direction θ_t. In that case, the received noiseless signal on one single reception antenna can be expressed as

$$y(t) = \sum_{m,r,h} e^{j\mathbf{x}_m^T \mathbf{k}(\theta_t)} c_{mh} e(t - hT_p - rT_h - \tau_t) e^{j2\pi\nu_t(hT_p + rT_h)} \tag{3}$$

where the three summations run for indices specified in Eq.(1) and (2), τ_t and ν_t are the target delay and Doppler frequency respectively, and we have assumed, as classically done in radar processing, that the phase rotation induced by the Doppler frequency is negligible over the pulse duration, thus resulting in a simple constant phase over T_p.

B. Matched filter for slow-time phase coding

As in classical radar processing, the well-known matched filter can be used at the reception to maximize the target Signal-to-Noise Ratio (SNR). This matched filter, considered as the solution of the Generalized Likelihood Ratio Test (GLRT) to the detection problem of a target with an unknown deterministic amplitude, consists in computing the scalar product between the received signal for a target with parameters $(\tau_t, \theta_t, \nu_t)$ and a model of the transmitted signal for hypothetic parameters (τ, θ, ν). Since the elementary pulse is the same for all time slots and antennas, the range matched filter can be performed as the convolution of the received signal with only $e(t)$, and we obtained the following matched filter output:

$$y_{mf}(\tau,\theta,\nu) = \overbrace{\sum_{r=0}^{N_r-1} \sum_{h=0}^{N_h-1} e^{-j2\pi\nu(hT_p+rT_h)}}^{\text{Doppler matched filter}} \times \underbrace{\sum_{m=0}^{N_T-1} e^{-j\mathbf{x}_m^T \mathbf{k}(\theta)}}_{\text{Tx beamforming}} \overbrace{c_{mh}^*}^{\text{phase code correction}} \underbrace{\int y(t) e^*(t-\tau)\, dt}_{\text{Range matched filter}}, \tag{4}$$

where $\cdot^*$ stands for the complex conjuguate.

The MIMO processing for slow-time phase codes can thus be viewed as the succession of the following steps:

- Range matched filter with the elementary pulse $e(t)$;
- Phase correction linked with the slow time phase code: it simply consists in multiplying each time slot of duration T_p with the corresponding conjugate phase c_{mh}^*;
- Angular transmission beamforming;
- Doppler matched filter over the whole pulse train, with a slow time step T_p.

Note first that, since the Doppler matched filter is performed over a duration $N_h N_r T_p$, the Doppler resolution is equal to $1/N_h N_r T_p$. Since the Doppler matched filter is performed with the slow time step T_p, the Doppler interval considered will be equal to $1/T_p$. Moreover the Doppler processing and the angular beamforming cannot be decoupled: indeed the presence of the phase terms c_{mh} mixes both Doppler (index h) and angle contributions (index m). This may create potentially strong Doppler/angle coupling, as illustrated in Figure 2 that represents the Doppler/angle cut for the delay τ_t of the matched filter output in presence of a single target. Finally the Doppler phase terms $e^{-j2\pi\nu r T_h}$ correspond to a pulse train with periodicity $T_h = N_h T_p$, and thus create an additional superimposed ambiguity pattern with period $1/N_h T_p$, that can be also observed in Figure 2.

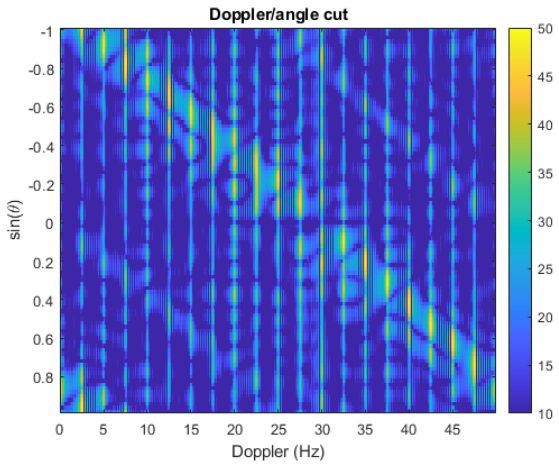

Fig. 2. Doppler/angle cut of the matched filter output for the delay τ_t of a target with parameters $\nu_t = 0$ Hz and $\theta_t = \pi/3$. Parameters of the STPC codes are provided in section V. Strong Doppler/angle coupling can be observed together with ambiguity pattern of period $1/N_h T_p$.

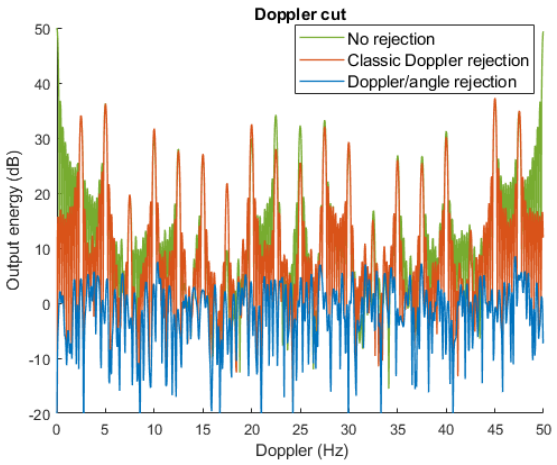

Fig. 3. Doppler cut of the matched filter output at the delay τ_c and angle θ_c of a 50 dB point-like clutter contribution with parameters $\nu_t = 0$ Hz and $\theta_t = \pi/3$. $N_T = 20$, $T_p = 10$ ms, Hadamard phase code of length $N_h = 20$.

This phenomenon is similar to the Doppler/angle coupling that is observed for Time Division Multiplex modulations proposed in low cost MIMO radar applications [9], but is induced here by the presence of the slow-time phase code. We will see in the following that this Doppler/angle coupling has a strong impact when Doppler rejection is performed.

III. Doppler/angle rejection for point-like clutter

In many radar applications, the presence of strong clutter echoes tends to deteriorate the detection performance. Since this clutter is usually located at a precise value in Doppler, the solution considered is often to remove all contributions corresponding to this Doppler shift in the received signal, for instance by least square rejection [16]: this consists in projecting the received signal orthogonally to the considered Doppler steering vector, for all range cell where some clutter is present. However, due to the potentially strong Doppler/angle coupling, this rejection must be carefully done: in particular one cannot simply apply classical Doppler rejection alone, as will be shown in the following.

In this section we will first consider the (not realistic) case of a point-like clutter, with parameters $(\tau_c, \theta_c, \nu_c)$. In that case, range compression to the received signal (3) for this clutter contribution provides the output

$$y_{rmf}(t) = \sum_{m,r,h} e^{j\mathbf{x}_m^T \mathbf{k}(\theta_c)} c_{mh} e^{j2\pi\nu_c q T_p} \Lambda(t - qT_p - \tau_c),$$

where $\Lambda(t)$ is the autocorrelation of elementary pulse $e(t)$ and $q = h + rN_h$. As in classical Doppler processing, considering the range cell τ_c (i.e. retrieving the signal samples at time $\tau_c + qT_p$ for $q \in [0, N_h N_r - 1]$), the clutter contribution in cell τ_c can be described by the vector $\mathbf{s}_{\theta_c,\nu_c}$ with entry $q = h + rN_h$

$$s_{\theta_c,\nu_c}(q) = \left(\sum_{m=0}^{N_T-1} e^{j\mathbf{x}_m^T \mathbf{k}(\theta_c)} c_{mh} e^{j2\pi\nu_c h T_p} \right) e^{j2\pi\nu_c r T_h}, \quad (5)$$

so that the noisy Doppler/angle received signal can be written

$$\mathbf{y}_{rmf} = A\mathbf{s}_{\theta_c,\nu_c} + \mathbf{n},$$

where A is an unknown deterministic complex amplitude and $\mathbf{n}$ is a zero-mean complex circular white gaussian noise.

Removing the clutter contribution here resorts to estimating the unknown amplitude A in the Maximum Likelihood sense, i.e. solving the very classic optimization problem [16], [17]

$$\hat{A} = \arg\min_A \|\mathbf{y}_{rmf} - A\mathbf{s}_{\theta_c,\nu_c}\|_2^2 = (\mathbf{s}_{\theta_c,\nu_c}^H \mathbf{s}_{\theta_c,\nu_c})^{-1} \mathbf{s}_{\theta_c,\nu_c}^H \mathbf{y}_{rmf},$$

and removing the corresponding contribution from $\mathbf{y}_{rmf}$, which consists in projecting the signal $\mathbf{y}_{rmf}$ orthogonally to the steering vector $\mathbf{s}_{\theta_c,\nu_c}$, resulting in the signal after rejection:

$$\mathbf{y}_{rej} = \mathbf{y}_{rmf} - \mathbf{s}_{\theta_c,\nu_c} (\mathbf{s}_{\theta_c,\nu_c}^H \mathbf{s}_{\theta_c,\nu_c})^{-1} \mathbf{s}_{\theta_c,\nu_c}^H \mathbf{y}_{rmf}. \quad (6)$$

Clearly from this expression, the orthogonal projector used for the rejection depends on both ν_c and θ_c. Thus, replacing in (6) the steering vector $\mathbf{s}_{\theta_c,\nu_c}$ by the classic Doppler steering vector $\mathbf{s}_{\nu_c}$ such that its k^{th} entry is $s_\nu(k) = e^{j2\pi\nu_c k T_p}$, would not remove perfectly the clutter contribution. In fact, it would remove all contributions at Doppler ν_c but not the Doppler/angle coupling induced by the STPC code. This can be observed in Figure 3 that presents the Doppler cut of the matched filter output at the delay τ_c and angle θ_c of a point-like clutter contribution. The Doppler cut without rejection shows strong ambiguities due to the phase code. Applying classic Doppler rejection enables to remove the clutter contribution at $\nu_c = 0$ Hz but the strong ambiguities remain. Applying the Doppler/angle projector provided by Eq.(6) enables to remove these strong ambiguities as well, and only noise remains here.

IV. Continuous angular rejection at constant Doppler hypothesis

In real applications, assuming that the clutter is located at a specific angular direction is not realistic. On the contrary, it is

usually spread over a wide angular area, while potentially being present only at specific frequencies. This is for instance the case for ground radar where the ground clutter will be located potentially in all angular directions but only at zero-Doppler, or for HFSWR radar [14] where the wave propagation along the sea surface creates Bragg peaks that correspond to two narrow frequency peaks present in any direction [12], [13]. It is then important to be able to remove these clutter contributions from the data in order to improve target detection.

Let us first assume that the continuous set of clutter angular directions to reject is discretized and thus corresponds to a set of N_θ directions $(\theta_i)_{i=1,\dots,N_\theta}$, so that the noisy Doppler/angle signal after range compression can now be written as

$$\mathbf{y}_{rmf} = \sum_{i=1}^{N_\theta} A_i \mathbf{s}_{\theta_i,\nu_c} + \mathbf{n},$$

and the orthogonal projector corresponding to these clutter contributions is provided by $\mathbf{P}_c = \mathbf{S}_c \left(\mathbf{S}_c^H \mathbf{S}_c\right)^{-1} \mathbf{S}_c^H$, where

$$\mathbf{S}_c = \left[\mathbf{s}_{\theta_1,\nu_c}, \mathbf{s}_{\theta_2,\nu_c}, \dots, \mathbf{s}_{\theta_{N_\theta},\nu_c}\right]$$

is a matrix of size $N_r N_h \times N_\theta$ that depends on the number of clutter contributions considered, and can thus be of very large size when finely discretizing the angular domain.

Fortunately this large matrix size can be dealt with by use of the Singular Value Decomposition (SVD) of the matrix $\mathbf{S}_c\mathbf{S}_c^H$. Indeed it is possible to show that the projector $\mathbf{P}_c$ can be written in the form [17]

$$\mathbf{P}_c = \mathbf{U}_S \mathbf{I}_M \mathbf{U}_S^H, \tag{7}$$

where $\mathbf{U}_S$ is provided by the SVD of $\mathbf{S}_c$ such that $\mathbf{S}_c = \mathbf{U}_S\mathbf{D}_S\mathbf{V}_S$ and $\mathbf{I}_M$ is the identity matrix where only the first M diagonal values are non zero, M being the number of non zero (or non negligible) singular values of $\mathbf{S}_c$. Thus the projector is fully described by M and $\mathbf{U}_S$. Noticing that $\mathbf{S}_c\mathbf{S}_c^H = \mathbf{U}_S\mathbf{D}_S^2\mathbf{U}_S^H$, it is then possible to obtain these quantities by computing the SVD of matrix $\mathbf{S}_c\mathbf{S}_c^H$, which is of size $N_rN_h \times N_rN_h$, independent of N_θ! It then suffices to compute this matrix $\mathbf{S}_c\mathbf{S}_c^H$ and the corresponding SVD.

Let us remark from the expression (5) of the Doppler/angle vector $\mathbf{s}_{\theta_i,\nu_c}$ that the matrix $\mathbf{S}_c$ can be decomposed in the form

$$\mathbf{S}_c = \mathbf{F}_{N_r}(\nu_c T_h) \otimes (\mathbf{C}_f \mathbf{X}),$$

where

- $\otimes$ denotes the Kronecker product;
- $\mathbf{X}$ is the matrix corresponding to the angular phase, whose (m,i) entry is given by $X(m,i) = e^{j\mathbf{x}_m^T\mathbf{k}(\theta_i)}$;
- $\mathbf{C}_f$ contains the phase code together with Doppler terms within the code duration N_h, whose (h,m) entry is provided by $C_f(h,m) = c_{mh}e^{j2\pi\nu_c h T_p}$;
- $\mathbf{F}_{N_r}(\alpha)$ is the vector of size N_r with terms defined by $(e^{j2\pi r\alpha})_{r=0,\dots,N_r-1}$.

Exploiting the properties of the Kronecker product and the particular sizes of the matrices involved here, we can write

$$\begin{aligned}\mathbf{S}_c\mathbf{S}_c^H &= \left[\mathbf{F}_{N_r}(\nu_c T_h) \otimes (\mathbf{C}_f\mathbf{X})\right]\left[\mathbf{F}_{N_r}(\nu_c T_h) \otimes (\mathbf{C}_f\mathbf{X})\right]^H \\ &= \left[\mathbf{F}_{N_r}(\nu_c T_h)\mathbf{F}_{N_r}^H(\nu_c T_h)\right] \otimes \left[\mathbf{C}_f\mathbf{X}\mathbf{X}^H\mathbf{C}_f^H\right]. \end{aligned} \tag{8}$$

Writing the following SVD of the two matrices in Eq.(8) as $\mathbf{F}_{N_r}(\nu_c T_h)\mathbf{F}_{N_r}^H(\nu_c T_h) = \mathbf{U}_F\mathbf{D}_F\mathbf{U}_F^H$ and $\mathbf{C}_f\mathbf{X}\mathbf{X}^H\mathbf{C}_f^H = \mathbf{U}_C\mathbf{D}_C\mathbf{U}_C^H$ and using the fact that the SVD of a Kronecker product is equal to the product of the SVDs enables to obtain

$$\mathbf{S}_c\mathbf{S}_c^H = (\mathbf{U}_F \otimes \mathbf{U}_C)(\mathbf{D}_F \otimes \mathbf{D}_C)(\mathbf{U}_F \otimes \mathbf{U}_C)^H, \tag{9}$$

and thus $\mathbf{U}_S = \mathbf{U}_F \otimes \mathbf{U}_C$. Thus computing the projector $\mathbf{P}_c$ only requires the computation of matrices $\mathbf{U}_F$ and $\mathbf{U}_C$.

Since $\mathbf{F}_{N_r}(\nu_c T_h)$ is a column vector, its SVD is straightforward, $\mathbf{D}_F$ only contains one non zero value associated to the normalized vector $\mathbf{F}_{N_r}(\nu_c T_h)/\|\mathbf{F}_{N_r}(\nu_c T_h)\|$ with $\|\mathbf{F}_{N_r}(\nu_c T_h)\| = \sqrt{N_r}$, and in fact in the computation we can even restrict $\mathbf{U}_F$ to this single normalized vector.

It suffices then to compute the SVD of matrix $\mathbf{C}_f\mathbf{X}\mathbf{X}^H\mathbf{C}_f^H$. Note here that $\mathbf{C}_f$ is of constant size $N_h \times N_T$. Although the matrix $\mathbf{X}$ is of size $N_T \times N_\theta$ and depends on the number of angular hypotheses, the matrix $\mathbf{X}\mathbf{X}^H$ is of constant size $N_T \times N_T$, and its (m,l) entry is provided by

$$\left(\mathbf{X}\mathbf{X}^H\right)_{m,l} = \sum_i e^{j\mathbf{x}_m^T\mathbf{k}(\theta_i)} e^{-j\mathbf{x}_l^T\mathbf{k}(\theta_i)}.$$

If we now assume that the angular hypotheses θ_i are uniformly distributed in $[\theta_{\min}, \theta_{\max}]$ with a sampling step $\Delta\theta$, and if we make $\Delta\theta$ tend towards 0 (and thus $N_\theta \to +\infty$), we obtain

$$(\mathbf{P}_\theta)_{m,l} = \lim_{\Delta\theta\to 0}\left(\mathbf{X}\mathbf{X}^H\right)_{m,l} = \int_{\theta_{\min}}^{\theta_{\max}} e^{j\mathbf{x}_m^T\mathbf{k}(\theta)} e^{-j\mathbf{x}_l^T\mathbf{k}(\theta)}\, d\theta. \tag{10}$$

Equation (10) provides the general expression for the projector over a continuous angular interval. In the particular case of a linear phased array with antennas separated by half the wavelength, this integral can be simplified. Indeed we classically get that $\mathbf{x}_m^T\mathbf{k}(\theta) = \pi m \sin\theta$ so that the angular phase is linear in $u = \sin\theta$. Considering then a sampling of the angular space in terms of u instead of θ, with bounds $u_{\min}$ and $u_{\max}$, we straightforwadly get the following projector

$$\begin{aligned}(\mathbf{P}_u)_{m,l} &= \int_{u_{\min}}^{u_{\max}} e^{j\pi m u} e^{-j\pi l u}\, du \\ &= e^{j\pi(m-l)\frac{u_{\min}+u_{\max}}{2}} \operatorname{sinc}\left((m-l)\frac{u_{\max}-u_{\min}}{2}\right).\end{aligned}$$

Such a matrix is well-known since it corresponds to the generating matrix of the Discrete Prolate Spheroidal Sequences (DPSS) [15], and we have already uncountered it in other applications ([18], [19] for instance).

It remains to compute numerically the SVD of matrix $\mathbf{C}_f\mathbf{P}_u\mathbf{C}_f^H$ of limited size $N_h \times N_h$ that enables to provide $\mathbf{U}_C$. Gathering (7) and (9) and restricting $\mathbf{U}_F$ to the normalized vector $\mathbf{F}_{N_r}(\nu_c T_h)/\sqrt{N_r}$ as previously mentioned, the projector $\mathbf{P}_c$ is finally provided by

$$\mathbf{P}_c = \frac{1}{N_r}(\mathbf{F}_{N_r}(\nu_c T_h) \otimes \mathbf{U}_C)\,\mathbf{I}_M\,(\mathbf{F}_{N_r}(\nu_c T_h) \otimes \mathbf{U}_C)^H,$$

with M the number of non-zero singular values of matrix $\mathbf{D}_c$.

V. Performance results

In this section, we present performance results obtained on simulated data. The considered MIMO array is a linear array with $N_T = 20$ antennas spaced by half the wavelength. The carrier frequency is $f_c = 6.5$ MHz, the chirp pulse has a bandwidth $B = 50$ kHz and a duration $T_p = 10$ ms. The STPC used is a Hadamard code of length $N_h = 20$, repeated $N_r = 10$ times, leading to 200 transmitted pulses for a total duration $T_{tot} = 2$s. Note that some parameters are not realistic for a HFSWR radar but chosen to ease the results presentation.

Two targets are simulated at respective approximate ranges 57 and 80 km, respective Doppler frequencies 11.7 and 7.3 Hz, respective SNR 25 and 20 dB, and an angle of $22.5°$ for both targets, the same angle being chosen to facilitate the result presentation. Clutter contributions are drawn as 10000 reflectors with the same Doppler frequency 2 Hz, ranges spanning the interval $[0, 100]$ km, and angles in $[-30°, 30°]$.

Since the matched filter output is 3-dimensional, we will only present either the range/Doppler cut obtained for the target angle (the same for both targets) or the angle/Doppler cut obtained for the range of the first target (57 km). We present in Figure 4 the range/Doppler cut obtained without and with the proposed Doppler/angle rejection method with $u_{\max} = -u_{\min} = \sin 30°$, and in Figure 5 the angle/Doppler cut in the same conditions. We clearly observe on the results before rejection the presence of clutter echoes that mask the targets, even though the clutter is located in the Doppler ambiguity interval $[0, 2.5]$ Hz and the two targets are located in different Doppler intervals. This is of course due to the strong STPC Doppler/angle coupling. After rejection, the target contributions can be clearly observed in Figure 4. The contribution of the first target with its Doppler/angle coupling is also visible in Figure 5, while the second target is less visible since the cut is not taken for this target range.

In order to better visualize the effect of the proposed Doppler/angle rejection method, we present in Figure 6 the angle/Doppler cuts for two different values of $u_{\max} - u_{\min}$, that is $u_{\max} = \sin 30°$ and $u_{\max} = \sin 15°$, the first one corresponding to the angular domain spanned by the clutter while the second one correspond to only half that angular domain. This figure presents zooms of the angle/Doppler cuts first for the Doppler ambiguity interval $[0, 2.5]$ Hz of the clutter, and second for the Doppler ambiguity interval $[10, 12.5]$ Hz of the first target. We can clearly see that for the interval $[0, 2.5]$ Hz the rejection method has indeed rejected contributions in the prescribed interval, so that when $u_{\max} = \sin 15°$ only the clutter contributions in that interval have been rejected. For $u_{\max} = \sin 30°$, all clutter contributions have been correctly rejected and the first target can be easily seen. In a similar way, in the interval $[10, 12.5]$ Hz, when rejection has only been performed for $u_{\max} = \sin 15°$, we can see the residual strong contribution of the clutter due to the Doppler/angle coupling, while it has been perfectly removed in case $u_{\max} = \sin 30°$. Note finally that in that case, no target would be detected at Doppler frequency 12 Hz that corresponds to an ambiguity of the clutter Doppler frequency, because the rejection removed all coupling contributions as well.

VI. Conclusion

In this article, we have considered the problem of Doppler and angle coupling in MIMO radar with STPC codes. We have shown that this coupling must be taken into account for Doppler rejection, and proposed a method that enables to reject clutter contributions at a fixed Doppler frequency over a given angular interval. This method enables to properly remove the clutter contribution and its Doppler/angle coupling. It could be used jointly with STPC codes optimized to limit the coupling. Further work shall be done to propose a method that enables to reject the clutter over a given 2D Doppler and angle patch.

References

[1] J. Bergin and J.R. Guerci. *MIMO Radar. Theory and Application*. Artech House, 2018.

[2] J. Li and P. Stoica. MIMO Radar with Colocated Antennas. *IEEE Signal Processing Magazine*, pages 106–114, 2007.

[3] B. Friedlander. Waveform Design for MIMO Radars. *IEEE Transactions on Aerospace and Electronic Systems*, 43(3):1227–1238, 2007.

[4] C. Chen and P. P. Vaidyanathan. MIMO Radar Waveform Optimization With Prior Information of the Extended Target and Clutter. *IEEE Transactions on Signal Processing*, 57(9):3533–3544, 2009.

[5] H. Deng, Z. Geng, and Himed B. MIMO radar waveform design for transmit beamforming and orthogonality. *IEEE Transactions on Aerospace and Electronic Systems*, 52(3):1421–1433, 2016.

[6] U. Tan, C. Adnet, O. Rabaste, F. Arlery, J.-P. Ovarlez, and J.-P. Guyvarch. Phase code optimization for coherent MIMO radar via a gradient descent. In *2016 IEEE Radar Conference*, pages 1–6, 2016.

[7] O. Rabaste, L. Savy, M. Cattenoz, and J.-P. Guyvarch. Signal Waveforms and Range/Angle Coupling in Coherent Colocated MIMO Radar. In *2013 International Conference on Radar*, 9 2013.

[8] K. Rambach and B. Yang. Direction of Arrival estimation of two moving targets using a time division multiplexed colocated MIMO radar. In *2014 IEEE Radar Conference*, pages 1118–1123, 2014.

[9] C. Hammes, M. R. Bhavani Shankar, and B. Ottersten. Generalized Multiplexed Waveform Design Framework for Cost-Optimized MIMO Radar. *IEEE Transactions on Signal Processing*, 69:88–102, 2021.

[10] Y. Tong and A. Tennant. A two-channel time modulated linear array with adaptive beamforming. *IEEE Transactions on Antennas and Propagation*, 60(1):141–147, 2012.

[11] D.J. Rabideau. Doppler-offset waveforms for MIMO radar. In *2011 IEEE RadarCon (RADAR)*, pages 965–970, 2011.

[12] B.J. Lipa and D.E. Barrick. Extraction of sea state from HF radar sea echo: Mathematical theory and modeling. *Radio Science*, 21(1):81–100, 1986.

[13] S. Grosdidier, P. Forget, Y. Barbin, and C.-A. Guérin. HF Bistatic ocean Doppler spectra: Simulation versus experimentation. *IEEE Transactions on Geoscience and Remote Sensing*, 52(4):2138–2148, 2014.

[14] F. Jangal and M. Menelle. French HFSWR contribution to the European integrated maritime surveillance system I2C. In *IET International Radar Conference 2015*, pages 1–5, 2015.

[15] D. Slepian. Prolate spheroidal wave functions, Fourier analysis, and uncertainty-V: The discrete case. *Bell System Technical Journal*, 57(5):1371–1430, 1978.

[16] F. Colone, D.W. O'Hagan, P. Lombardo, and C.J. Baker. A Multistage Processing Algorithm for Disturbance Removal and Target Detection in Passive Bistatic Radar. *IEEE Transactions on aerospace and electronic systems*, 45(2):698–722, 2009.

[17] O. Rabaste and D. Poullin. Rejection of Doppler Shifted Multipaths in Airborne Passive Radar. In *IEEE International Radar Conference 2015*, pages 1660–1665, 5 2015.

[18] J. Bosse, O. Rabaste, and D. Poullin. Matching Pursuit via Continuous Resolution Cell Rejection in Presence of Unresolved Radar Targets. In *EUSIPCO 2015*, 2015.

[19] O. Rabaste and J. Bosse. Robust Mismatched Filter for Off-Grid Target. *IEEE Signal Processing Letters*, 26:1147–1151, 2019.

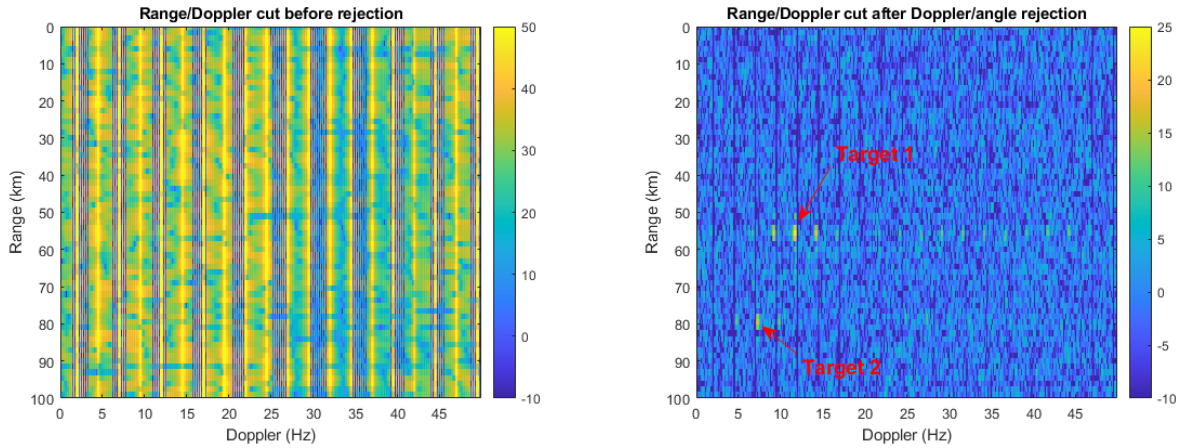

Fig. 4. Range/Doppler cut of the matched filter output for the angle of the targets. Left: before rejection. Right: after Doppler/angle rejection. Although the strong Doppler/angle coupling created by the clutter prevents from detecting the targets before rejection, they can be easily detected after rejection.

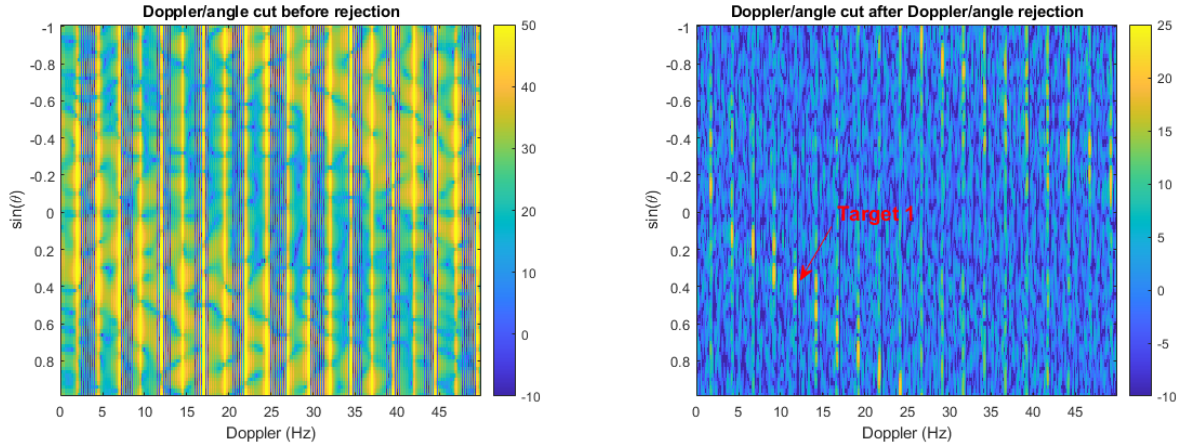

Fig. 5. Angle/Doppler cut of the matched filter output for the range of the first target. Left: before rejection. Right: after Doppler/angle rejection. Again the proposed Doppler/angle rejection has enabled to remove the clutter contribution, and target 1 can be detected in that range, together with its Doppler/angle coupling (target 2 is not in the same range cell, but some coupling contribution can still be observed).

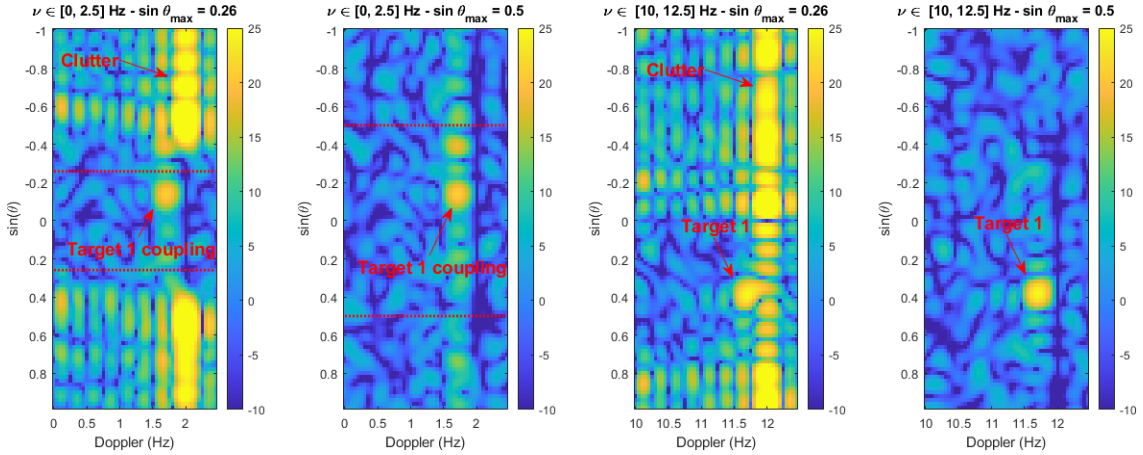

Fig. 6. Angle/Doppler cut of the matched filter output for the range of the first target for the Doppler ambiguity of the clutter (interval $[0, 2.5]$ Hz, two left figures) and for the Doppler ambiguity of the first target (interval $[10, 12.5]$ Hz, two right figures). Two angular interval have been considered for the rejection: $u_{\max} = \sin 15°$ (first and third subfigures), and $u_{\max} = \sin 30°$ (second and fourth subfigures). In third subfigure where all clutter contributions have not been fully removed, the target contribution is partially masked by the clutter residual Doppler/angle coupling. The dashed lines in the two first figures represent the angular interval for the rejection for the Doppler frequency of the clutter.